A facility for cryogenic ion irradiation and *in situ* characterization of Rare-Earth Barium Copper Oxide superconducting tapes

A. Devitre,[1] D.X. Fischer,[1] K.B. Woller,[1] B.C. Clark,[1] M.P. Short,[1] D.G. Whyte,[1] and Z.S. Hartwig[1]
Plasma Science & Fusion Center, Massachusetts Institute of Technology, 02139 Cambridge, Massachusetts, United States

(*Electronic mail: devitre@mit.edu, dafisch@mit.edu)

(Dated: 21 April 2024)

Superconducting magnets based on Rare Earth Barium Copper Oxides (REBCO) offer transformative capabilities in the fields of fusion energy, high energy physics, and space exploration. A challenge shared by these applications is the limited lifetime of REBCO due to radiation damage sustained during operation. Here we present a new ion-beam facility that enables simultaneous cryogenic irradiation and *in situ* characterization of commercial REBCO tapes. The ion source provides spatially uniform fluxes up to 10^{19} protons/m^{2}s with kinetic energies up to 3.4 MeV; in addition to helium and higher-Z species. Using this facility, we can induce uniform damage profiles in the first 10-20 μm of REBCO tapes with less than 0.25 appm of hydrogen implanted in REBCO after a dose of 10^{20}protons/m^2. The tape can be held at 20-300 K with an accuracy of $\pm$ 0.1 K, and is connected to a four-point probe measuring the critical current, I_c, and critical temperature, T_c, before, during, and after irradiation with transport current ranging from 100 nA to 100 A, and a typical voltage noise less than 0.1 μV. These capabilities are presently used to study the effect of irradiation temperature on REBCO performance change during and after proton bombardment, to assess the possibility of I_c and T_c recovery after irradiation through thermal annealing, and to explore the instantaneous and recoverable suppression of I_c and T_c observed during irradiation.

I. INTRODUCTION

Large-scale superconducting magnets have been an important enabling technology in science and industry since the 1960s, when low temperature superconductors like NbTi and Nb_3Sn began displacing resistive copper magnets in a number of applications such as medical imaging, particle accelerators, and fusion energy devices. The advantages of superconducting magnets in these applications are twofold: first, significantly lower power consumption, which reduces operating cost, and second, access to much higher magnetic fields, which opens up new scientific and practical capabilities. The discovery and industrial production[1] of rare earth barium copper oxides (REBCO) have enabled research and development towards a new generation of large-scale magnets operating well in excess of 15 T. The impacts of such magnets on the fields of fusion energy, high energy physics (HEP), nuclear medicine, and space applications, in particular, are transformative. For magnetic-fusion devices, key metrics of performance scale non-linearly with the magnetic field, B, confining the thermonuclear plasma. For example, the tokamak's fusion power density scales like B^4, which provides the ability to dramatically reduce the size, cost, and time-to-build fusion power plants by using high-field REBCO magnets[2]. Favorable scalings coupled to the maturation of REBCO-magnet technology have led recent efforts to accelerate the commercialization of fusion energy by integrating high-field REBCO magnets into compact fusion energy devices such as tokamaks[3,4], stellarators[5], and magnetic mirrors[6]. Similarly, in HEP experiments, increasing the magnetic field plays a pivotal role in reducing the diameter of the collider ring. In order to expand the energy frontier beyond the 14 TeV available at CERN's Large Hadron Collider, increasingly higher magnetic fields will be required to enable practical costs, siting, and construction of such devices. For aerospace applications, the ability to produce high magnetic fields at low power and small mass enables new concepts for radiation shielding of astronauts and electronics[7], lunar magnetic energy storage in permanently shadowed regions[8], and long-lived, enhanced-maneuverability thrusters for satellites and deep-space.

A common unifying theme for these applications is that the superconductor is exposed to ionizing radiation fields during operation. Over prolonged periods of time, microstructural changes induced by radiation damage degrade the ability of the magnet to carry current without resistance and, hence, its ability to produce the desired magnetic field. Strategies for mitigation are expensive and time-consuming, requiring costly upfront design and fabrication decisions, or wholesale replacement of the magnets. For example, conceptual design studies of future fusion energy power plants[9] and next-generation colliders[10] identify the superconducting magnets as the dominant technical cost and schedule driver for new facilities. Thus, understanding the radiation tolerance of magnets in these machines becomes necessary for proper design, accurate costing, and successful operation.

In these devices, magnets operate under a complex set of physical conditions, each of which can influence the response of REBCO to radiation. These include cryogenic temperatures, immersion in a high magnetic field, and the transport of electrical current. Due to the challenge of replicating these conditions within a laboratory-based radiation facility, almost all data on radiation damage in commercial REBCO coated conductors has been acquired following irradiation at or above room temperature ($T_{irr} \geq$ 293 K), in self-field (B$\sim$0 T), and without transport current, leaving large uncertainties about how these results translate to the operation of REBCO under irradiation at 4-20 K in a 10-20 T magnetic field.

To address this shortcoming, we have developed an ion-beam facility for the irradiation REBCO coated conductors at cryogenic temperatures, imparting the ability to measure the superconducting properties before, during, and after irra-

diation. We describe the major elements of this facility and present a series of initial tests results. These data validate the capabilities of our facility and reveal a thermal-annealing recovery of the superconducting properties starting well below room-temperature.

II. RADIATION DAMAGE IN REBCO

A. A short review of superconductivity

Superconductivity is a thermodynamic state characterized by positive interactions between electrons (Cooper pairs), enabling near-zero electrical resistance[11,12]. Cooper-pairs form when temperature drops below the critical temperature, T_c, and break if the ambient magnetic field is too high. The loss-free transport of current, in technical superconductors, is based on a phenomenon called flux pinning[13]. Above the lower critical field H_{c1}, magnetic flux enters the bulk of the material as vortices, consisting of a normal-conducting cores surrounded by screening currents. It follows that any applied transport current, I_{op}, flowing through the material causes a Lorentz force $F_l \propto I_{op} \times B$ acting on the vortices. Below a certain critical current, I_c, the Lorentz force is counteracted by the pinning force F_p, arising from spatial variations in Cooper pair density (or pinning potential) within the unit cell, or at lattice defects. Above I_c, $F_l > F_p$; the vortices are no longer pinned and start moving. An electric field appears, causing electrical resistance. The relationship between the emerging electric field, E, and I_{op} can be described by a power law

$$E(I_{op}) = E_c \left(\frac{I_{op}}{I_c} \right)^n \tag{1}$$

which defines I_c through the conventional[14] electric-field criterion $E_c = 1\,\mu V/cm$. The exponent, n, describes the sharpness of the transition from the loss-free to resistive state. While the mechanism for Cooper pair formation in the cuprates remains a mystery[12], radiation has been used to modify the pinning landscape of superconductors and evaluate the consequences of different microstructures on superconductivity[15].

B. Radiation-induced defects in REBCO

There is a large body of literature on the irradiation of REBCO with gamma photons[16], electrons[17], neutrons[18], protons[9], and heavy ions[19]. Gamma and other photon irradiations have repeatedly shown little to no effect on the superconducting properties, including recent cryogenic-irradiations with *in situ* transport measurements[16]. While electrons at MeV energies only produce isolated vacancy-interstitial pairs, neutrons and ions can also create collision cascades, clusters, and amorphized tracks[20].

The larger defects have long been observed with transmission electron microscopy (TEM)[21]. Most recently, Linden[22] imaged the REBCO layer of coated-conductors irradiated in a fission reactor-core, where the thermal neutron spectrum was shielded by a cadmium foil. They found evidence of collision cascades in the form of 2 to 3 nm amorphous regions surrounded by a strain field about double the size. These large defects were stable up to 575 K.

Point defects, on the other hand, have not been observed directly. Their presence can be inferred, as we will show, from the recovery of I_c and T_c observed after annealing in cryogenically irradiated tapes. With prolonged irradiation, the accumulation of point defects and small clusters reduces T_c by scattering superconducting charge carriers. However, the mechanism for I_c degradation is not well-understood: a moderate increase in the defect density can enhance I_c–especially in an external magnetic field–by improving flux pinning, but large defect concentrations will decrease I_c[18], likely due to a decreasing Cooper pair density[15].

Unraveling the structure-to-property relation requires the characterization of radiation-induced pinning-landscapes and their effect on superconducting properties. The first step is to develop a facility to irradiate and measure the properties of REBCO tapes at cryogenic temperatures, with the option to apply an external magnetic field. From there, microstructural analysis tools should be added to identify the relevant defects and quantify their accumulation in magnet-operating conditions. For example, the irradiated REBCO tapes could be transferred in liquid nitrogen to an advanced electron microscope with sufficient resolution to resolve the structure of the oxygen sub-lattice[23], or to a synchrotron for chemical analysis[24]. The size distribution and concentration of open-volume defects, as well as their location within the unit cell, could be determined with a slow-positron beam equipped with lifetime and Doppler-broadening detectors[25,26]. Such a device, coupled to a cryogenic irradiation target capable of measuring I_c, T_c, and the density of charge carriers *in situ*, would provide a direct relation between microstructural changes and the performance degradation of REBCO tapes.

C. Existing facilities for the irradiation of coated superconductors at cryogenic temperatures

An ideal facility to explore radiation effects in superconducting REBCO magnets should have the ability to directly characterize I_c and T_c at relevant magnet operating temperatures and magnetic fields (magnitude and direction). The nature of the incident particles and their energy spectrum should match the conditions of the application. The achievable dose should be commensurate with the expected lifetime of the magnet. The capability to measure I_c and T_c *in situ* – while maintaining cryogenic temperatures between irradiation and measurement – is necessary to capture the evolution of an irradiated magnet during long-periods of operation, and isolate the effect of magnet warm-up during maintenance. The capability to measure I_c and T_c *in operando* – with transporting current during irradiation – is essential to characterize the behavior of the superconductor during operation. Historically, few experiments have incorporated all of these capabilities at once. Here we review two classes of such facilities: neu-

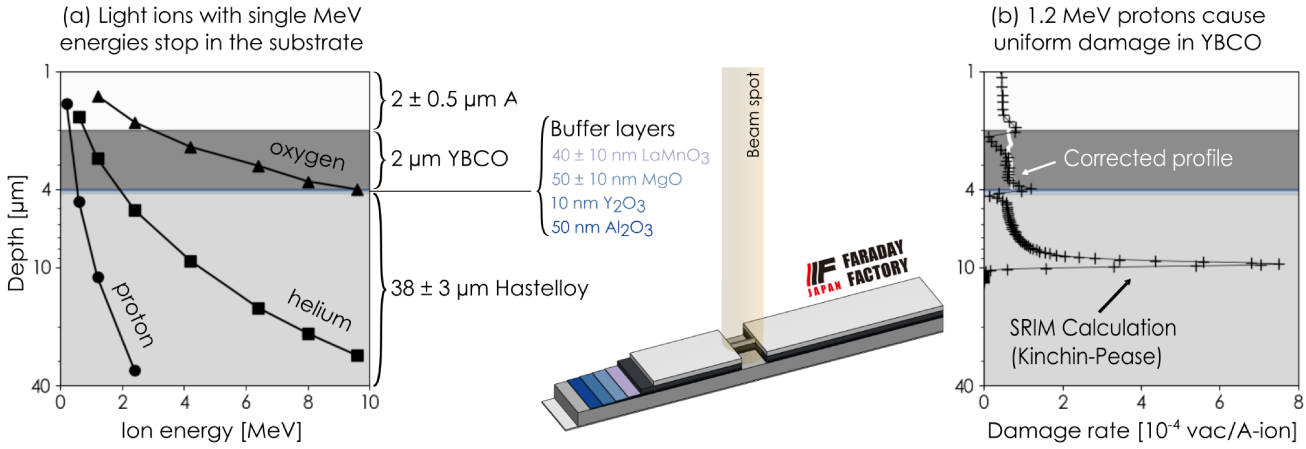

FIG. 1. Calculations of ion implantation depth and the damage profile caused by light ions with single MeV energies show that there is (a) little to no implantation of protons in the REBCO layer and (b) a uniform, neutron-like, damage profile.

tron irradiation in or next to experimental fission reactors; and charged particle irradiation on accelerator beam lines.

Fission reactor[27] and spallation[28] neutron irradiation present two main challenges: the first is a mismatch between the intermediate energies present in fusion or HEP magnets, and the slow-to-thermal (fission) or very fast (spallation) neutron energy spectra. The second relates to space and regulatory constraints, as well as high nuclear and conductive loads. Despite these challenges, cryogenic neutron irradiation of thin REBCO films and bulk specimens were performed at three facilities in the late 1980s and early 1990s. The low-temperature irradiation loop at Kyoto University[29] was used to irradiate REBCO at 20 K up to a dose of 2×10^{20} neutrons/m^2, too low to observe any change in T_c. Researchers at the Munich research reactor[30,31] achieved a much higher fast neutron fluence of 9×10^{22} n/m^2 at 15 K. They observed about 50% T_c degradation, but did not publish annealing data. A team at the Institute for Metal Physics in Russia[32] irradiated REBCO at 80 K up to 10^{23} n/m^2. They did not measure T_c *in situ*, but they observed an additional recovery of T_c after two weeks at 300 K, compared to T_c measured 20 minutes after warm-up. To our knowledge, there was only one successful cold sample transfer[33] to an external measurement setup ($T < 77$ K) following a cryogenic irradiation ($T \sim 4.6$ K). It revealed changes in I_c as a function of temperature and magnetic field up to 8 T.

In contrast to neutron experiments, charged particle facilities offer significant flexibility, particularly for the implementation of a cryogenic irradiation target. Here the challenge is to maintain excellent temperature control of the samples during irradiation, through careful engineering of the target holder. For instance, Coulomb collisions between incident ions and lattice atoms can cause local heating in the superconducting layer up to several GW/m^3. Researchers at the Karlsruhe Institute of Technology irradiated REBCO thin-films as early as the late 1980s. These 800 nm thick films were irradiated at 77 K with 300 keV He to a fluence of 2×10^{20} ions/m^2, which completely amorphized the lattice structure[34]. More recently, in 2017, Sorbom irradiated commercial REBCO tapes with protons at 80 K, 323 K, and 423 K. These experiments identified differences in degradation rate and field-angle dependence of I_c as a function of irradiation temperature[35]. The ion irradiation experiment presented in this article extends the capabilities developed by Sorbom. First commissioned in January 2020, this new facility allows (i) a gradual increase of sample temperature after irradiation; (ii) the measurement of I_c and T_c during irradiation; and (iii) the use of different ion-beam species. A comparable setup was since developed and operated at the Surrey ion-beam laboratory in the UK[36].

III. EXPERIMENTAL EQUIPMENT AND METHODS

A. REBCO coated-conductor samples

Coated conductors, also known as 'tapes', are materials of various layer-thicknesses and compositions. Figure 1, for example, shows the tape composition of Faraday Factory Japan[1]: 2 μm of YBCO with dispersed Y_2O_3 nanoparticles capped by 2 μm of silver. A Hastelloy substrate (38 $\pm$ 3 μm) provides mechanical stability over the wide range of temperatures experienced by the tape. The buffer facilitates a bi-axial growth of the REBCO layer, warranting low angles between grains, allowing high critical currents[37]. Off the shelf tapes also include a copper jacket, surrounding the stack, to help temperature stability and current distribution in cables. But our tapes were procured without stabilizer, such that light ions with single MeV energies can produce a uniform damage profile in the REBCO layer and implant several microns into the substrate.

The cryogenic target holder accommodates 3-6 cm long samples of REBCO tape, compatible with the magnet bore diameter of many high-field characterization facilities[15,38]. Halfway along the tape, the 4 mm width is reduced to a 0.1 mm bridge: the silver, REBCO, and buffers are ablated on both side of the bridge, leaving the substrate exposed. Bridging tapes has several advantages:

- 40x less transport current needed to measure I_c.
- Lower transport currents cause less Joule heating $\propto I^2$.
- A bridge length $l = 2$ mm, yields a well-defined voltage criterion $V(I_c) = V_c = E_c l = 0.2\mu V$.
- The properties of the tape are determined by the bridge, which reduces the beam spot size needed to irradiate homogeneously and allows for higher ion fluxes.

Custom bridge patterns are programmed in the SCAPS SAMLight control software and engraved by a Bright Solutions Wedge XF 532 OEM Integrated Marker, operating at 80 W and 50 kHz, scanning at a speed of 200 mm/s. A recent Masters thesis compares the laser-skiving technique to the more common chemical etching and photolithographic process. Several bridge patterns were tested between 4 and 77.3 K, in magnetic fields up to 20 T, finding that microbridges with widths ranging from 40 to 400 μm retained a larger fraction of the full tape n-value and critical current, as compared to chemically etched bridges of the same width[39].

B. Ion accelerator, beamline, and irradiation chamber

The ion source is a General Ionix 1.7 MV tandem accelerator operated at the MIT CLASS accelerator laboratory. The accelerator provides proton beam-currents from a few nA up to tens of μA, which can be kept within $\pm$ 1% for several hours of irradiation. This allows uniform beam current density up to 10^{19} ions/m^{2}s on sample. The ion beam is extracted from the accelerator column and magnetically steered onto the target holder, attached to cold head, at the end of the beamline. The beamline, shown in figure 2, contains instrumentation and diagnostics to measure the beam current and maintain its spatial uniformity. An upstream quadrupole magnet shapes the beam into a Gaussian profile, with a FWHM larger than the aperture of the collimator. This provision constrains flux uniformity (dose rate) to a factor of two. While the results presented below use 1.2 MeV protons as a proxy to fusion neutrons at the magnets of an ARC-class reactor[9], the ion source can produce a variety of light and heavy ions, including He, O, Si, and most transition metals. The maximum kinetic energy of a given ion-beam species $E_{beam} = 2qV_{ter} + V_{ext}$ depends on its charge-state, q, the source extraction voltage, V_{ext}, and the terminal potential V_{ter}. The value of V_{ter}, and thus E_{beam}, is known with a precision of $\pm$ 5 kV. Meanwhile, the maximum achievable beam current depends on the production of the desired ion charge state by charge-exchange at the terminal, where negatively-charged ions are stripped of their electrons by nitrogen gas.

C. Target holder design and implementation

The cryogenic target holder, shown in figure 3, is assembled outside the irradiation chamber and attached to the cold head via mounting screws. Its design fulfils, in particular, three major requirements:

1. Temperature control between 20 and 300 $\pm$0.1 K.
2. Uniform irradiation of the REBCO layer, with a flux uncertainty less than 1 nA $\sim 10^{15}$protons/m^{2}s.
3. Measurement of I_c and T_c during and after irradiation with a voltage noise level $\delta V \leq 0.1\ \mu V$.

1. *Irradiation target holder cryogenic design*

The target holder is designed to maximize heat conduction while minimizing thermal radiation and Joule heating. Convective heat transfer between the cold mass and the chamber walls is largely suppressed by vacuum in the accelerator, where pressure remains under 5×10^{-6} Torr. The system is cooled from room temperature to 20 K in less than 2 h by a Cryomech AL-230 cold head, with 25 W of cooling power at 20 K and a base temperature of 15 K. Heating is provided by four parallel cartridge heaters, contributing a total of 400 W. The heaters are driven by a Sorensen DCS 150-7E power supply regulated by a Lakeshore 336 temperature controller, which reads temperature from a sensor embedded in the cold head amidst the heaters (CX-CH). To maintain thermal contact through temperature cycles and compensate for different thermal contractions, all bolts are spring-loaded with Inconel 718 Belleville washers. Metal oxides are eliminated from all interfaces with solder flux and organic solvents, and the contact surfaces are lined with cryogenic grease. The N-Apiezon grease also minimizes the impact of surface roughness on heat conduction. A thin layer of indium ($\sim 5\ \mu$m) is preferred to grease where a fast thermal response (e.g., temperature sensors) or a good electrical connection (e.g., terminal blocks) is required. To avoid conducting heat from the feedthroughs to the tape, we use Lakeshore Quad-Lead cryogenic wire (WQL-36) for Cernox sensors, Twisted lead wire (WCT-34) for voltage probes, and AWG 12 copper wires for current leads soldered to the terminal blocks. All wires are also thermally anchored to the cold head.

A suite of three Cernox sensors is used to monitor the temperature on the target holder. The first is attached to the thermal shield (CX-S), and used to quantify radiative heat load. To minimize thermal radiation, the inner walls of the target chamber were covered with 24 sheets of multilayer insulation; except for the beam port and a 2-3/4" view-port used to image the beam fluorescence on the collimator. Any remaining thermal radiation is directly coupled to the heat sink by a radiation shield. The remaining heat load (either conducted by the cables or radiated by the shield) can be inferred by the heating power required to maintain the temperature at 20 K compared to the nominal 25 W of cooling provided by the cold head.

The second Cernox sensor is affixed to the positive terminal block (CX-TB). This excludes any heat conducted by the current leads, e.g., poor thermal anchoring or Joule heating during transport measurements. If Joule heating is observed, the size of the current step is increased such that the system spends less time at high current. This ensures that the I-V curve is not distorted by a temperature increase.

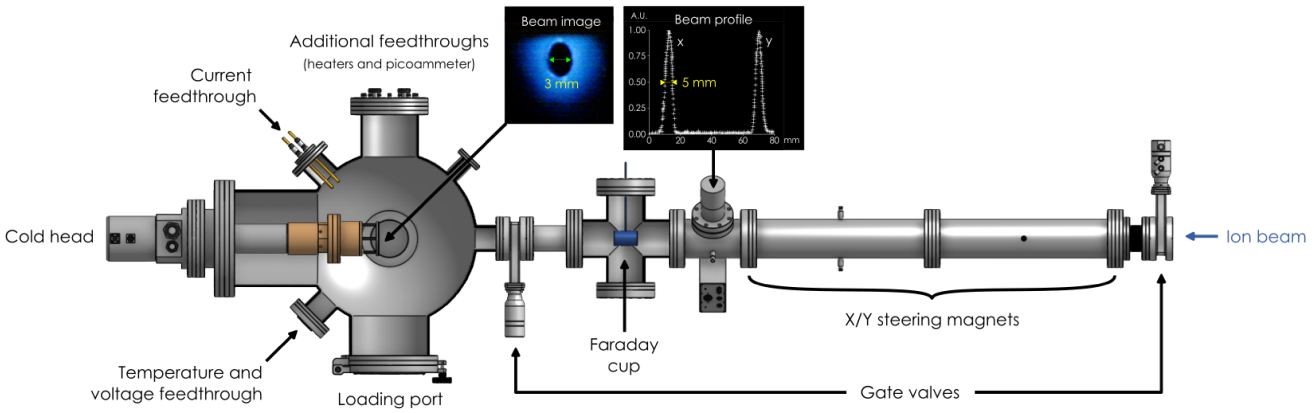

FIG. 2. The beamline and irradiation chamber of the cryogenic irradiation facility contain a set of diagnostics and actuators to maintain the intensity and spacial uniformity of the beam current. An upstream quadrupole magnet (not shown) is used to shape the beam, which can be imaged on the borosilicate glass collimator (by scintillation) and the beam profile monitor (by sampling charge).

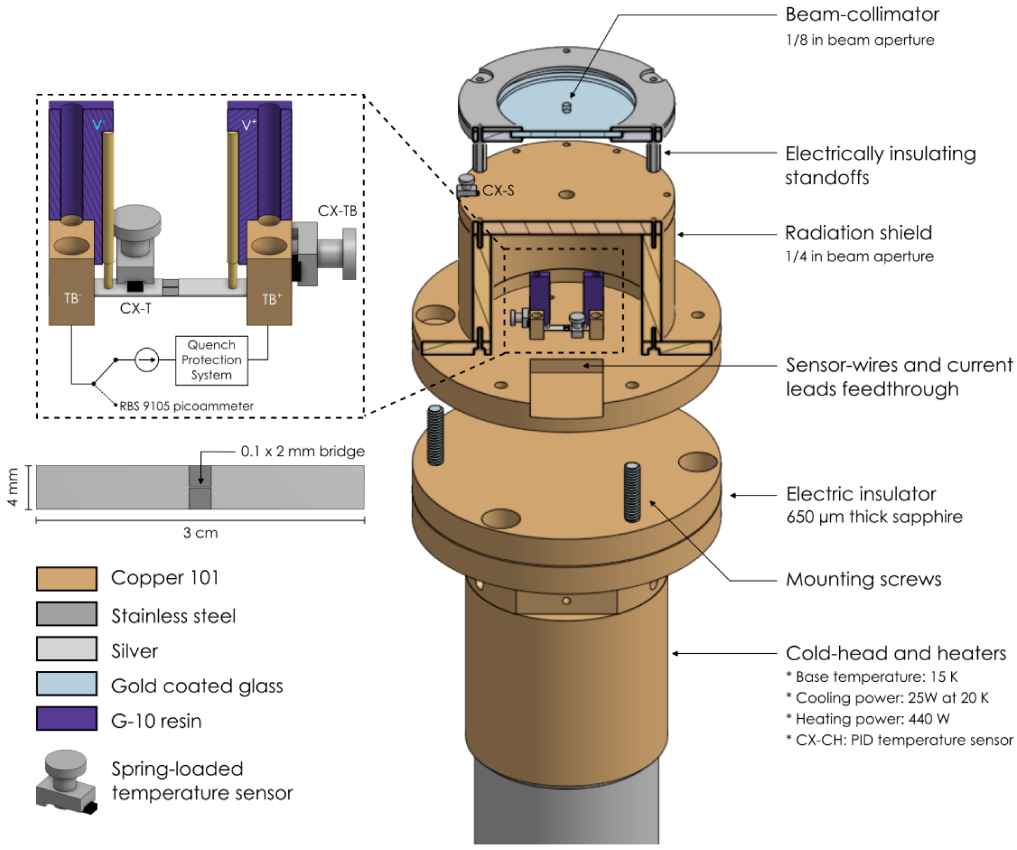

FIG. 3. The cryogenic target assembly, made of copper and sapphire, (i) controls the sample temperature between 20 and 300 K; (ii) measures the superconducting properties of REBCO tapes during and after irradiation; and (iii) collects the beam current deposited on target as a measure of dose. The bridge pattern, engraved in the tape, reduces the current-limiting section of the tape to a 2 x 0.1 mm segment.

Fluence	x^3	x^2	x	1
0e00 m^{-2}	-2.28e-07	6.80e-05	-0.0086	0.34
6e20 m^{-2}	-1.43e-06	4.21e-04	-0.0526	2.06

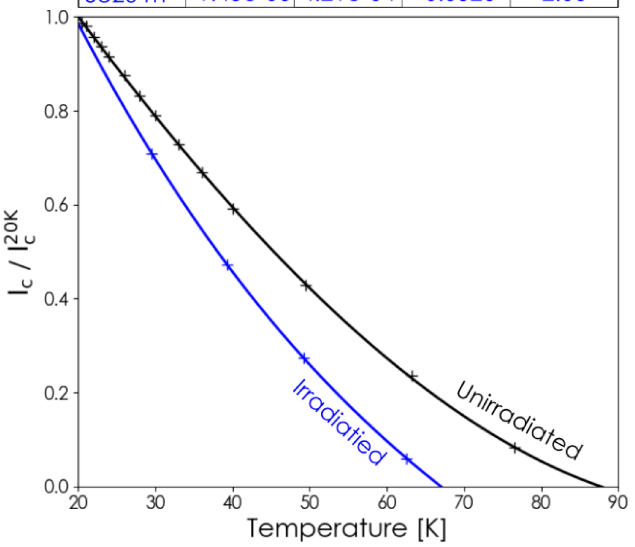

FIG. 4. In the 20 to 30 K range, a 0.4 K difference causes a 1% change in I_c. The sensitivity of I_c increases after irradiation, whereby 1% change happens for a 0.3 K difference. The table provides coefficients of a third-order polynomial fit. Each marker is the average of 3 measurements and the error bars are smaller than the markers.

With these provisions, sensor CX-TB agrees with sensor CX-T–pressed against the surface of the tape, approximately 4 mm away from the center of the beam spot–within their typical fluctuations ($\pm$0.1K) over the range of 20-300 K. This bounds the temperature of REBCO, and sets the maximum accuracy to which we can determine T_c and I_c. As shown in figure 4, a 0.4 K difference at about 20 K causes a 1% change in I_c. Sensors CX-TB and CX-T typically differ from CX-CH by less than 1 K, which is evidence for heat carried into the system by the current leads. A future upgrade of the facility thus foresees the use of superconducting current leads, to eliminate Joule and conductive heat loads. The accuracy of CX-T is routinely cross-checked by comparing I-V curves measured in a bath of liquid nitrogen to those taken *in situ* at 77.3 K. The *ex situ* test station uses the same set of electronics and power supplies as the target holder, and provides a quick check before mounting a sample to the target holder.

During experiments, we observed that the temperature of the tape (CX-T) rise and fall as we steered the beam on and off sample. This suggests ion beam heating but cannot be verified directly; adding a sensor in the irradiated area would block the beam. Therefore, we used the temperature dependence of Ic, obtained in thermal equilibrium, without the beam, to infer the temperature of the REBCO layer during irradiation. This experiment, showcased in figure 5, points to an $\sim$ 8 K gradient between the REBCO layer and the CX-T sensor for a 30 nA proton beam with an energy of 1.2 MeV. However, this conclusion is only valid if the suppression of I_c, measured during irradiation, is a predominantly thermal effect.

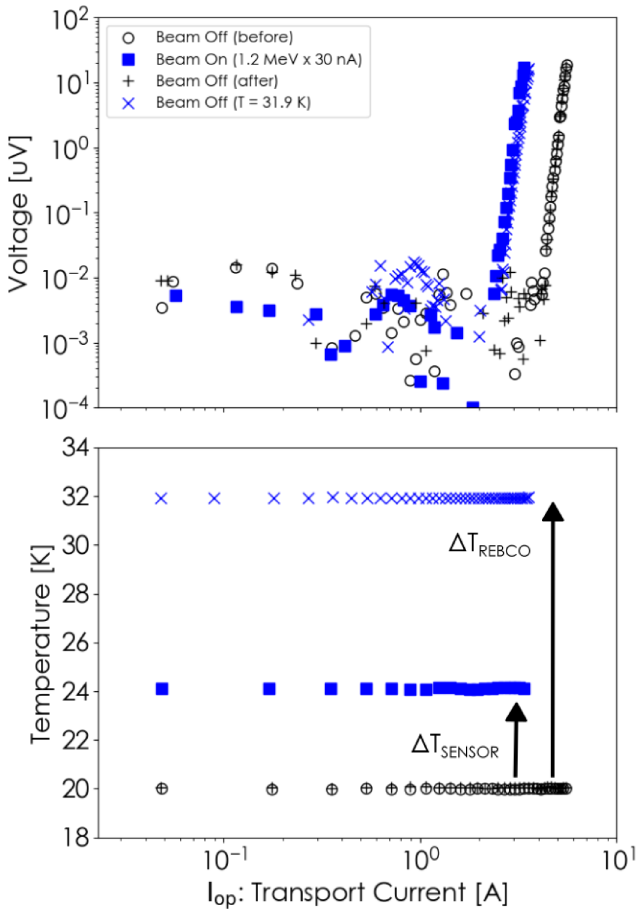

FIG. 5. The temperature needed to match the beam off curve (×) to the beam on curve (■) suggests an 8 K gradient between the REBCO layer under irradiation (ΔT_{REBCO}) and temperature sensor CX-T (ΔT_{SENSOR}), located 4 mm away from the center of the beam spot.

2. *Online beam current measurements*

Accurately quantifying dose requires a precise account of incident particles per unit area, or fluence. Fluence is measured by tallying the charge deposited by the beam on the target holder with a picoammeter, connected to the positive terminal block by a relay. The RBD-950 picoammeter can measure beam currents with sub-nA resolution and provides a 90 V bias to prevent the loss of charge caused by secondary electron emission when the beam hits the target. We find, however, that secondary electron suppression is not needed since the radiation shield acts as a Faraday cage for the electrons. For a homogeneous beam current density, fluence is then a simple time integral of beam current:

$$\Phi\left[\frac{\text{protons}}{\text{m}^2}\right] = \frac{4}{Ze\pi d^2}\int \text{dt}\, I_b(t) \qquad (2)$$

where $I_b(t)$ is the ion beam current measured in nA, Z is the charge of the incident ion, e is the elementary charge. For a 1/8 inch diameter collimator, d, the constant preceding the integral is $\sim 7.9\times10^{14}$protons/nA-m^2.

Fluence measurements can provide an estimate of primary radiation damage, reported as the a number of displacements per atom (dpa) in the irradiated volume. While dpa is a calculated quantity, which depends on a displacement model—and does not consider the evolution of defects beyond the initial stages of the damage cascade—it is a necessary step to compare radiation effects across incident particle species and energies. The gold standard for dpa calculations is a Monte Carlo code known as the Stopping Range of Ions in Matter (SRIM), which implements the NRT model under the binary collision approximation[40]. But SRIM has known (and often overlooked!) issues and numerical artefacts. For example, the peaks and troughs featured at the layer boundaries in figure 1 are caused by the free-flight approximation, used in both Kinchin-Pease and Full Cascade calculations. The SRIM documentation suggests that "you do not worry about small peaks and dips at layer edges, they are not worth the trouble to try to avoid, and just average the final curves"[40]. However, for the case of coated conductors, these features are large, and it is not obvious that averaging would produce meaningful results. Instead, we repeated the calculation for 1.0 MeV protons impacting a pure YBCO target, accounting for the energy lost to the silver layer. The resulting 'corrected' profile, is compared to the full-tape calculation in figure 1 showing good agreement away from the layer boundaries, and a linear slope that is consistent with uniform stopping power through a homogeneous material. A lesser-known issue is that the random seed of the Monte-Carlo simulation is only set once, and repeats itself every 50k ions[41]. To obtain sufficient statistics (typically 300k ions and above for displacements), it was therefore necessary to restart the calculation periodically, and average the results of several runs. Under these conditions, SRIM provides an average number of vacancies/Å-ion, K_{SRIM}, that can be used to convert from fluence to dpa:

$$[\text{dpa}] = \frac{K_{SRIM}}{N_{YBCO}} \Phi \tag{3}$$

where $N_{YBCO} \approx 7.5 \times 10^{28}$ atoms/m^3, and $K_{SRIM} = K_{PKA} + K_{recoils}$, calculated for 1.2 MeV protons incident on a Faraday Factory tape. This ratio is $\sim 2.8 \times 10^{-24}$ using the Kinchin-Pease displacement model.

Repeatability is a common issue when comparing the results of irradiation experiments. Aside from sample-to-sample variations, discrepancies arise from spatial and temporal inhomogeneities in the ion-beam flux density. Such dose rate variations can confound irradiation results in several ways. Inhomogeneous or slowly rastered beams can change the point-defect kinetics over the irradiated area, causing neighboring regions to evolve asynchronously[20]. In our setup, the beam is shaped into a Gaussian profile with a FWHM equal or larger than the 1/8 in. pinhole of the gold-coated glass collimator using a quadrupole and a beam-profile monitor. The gold coating is regularly refreshed to ensure that the accumulated charge can be exhausted through a grounding wire. Otherwise arcing occurs, which can destabilize the beam causing large variations in the beam current measured on the tape.

Inhomogeneous damage also happens as a function of depth. Since ions interact with lattice atoms by Coulomb scattering, the damage profile peaks where the ion has lost most of its energy. This region, known as the Bragg peak, is characterized by a steep gradient in dose rate and a large number of implanted interstitials. Torsello et al. showed that a shallow Bragg peak within the substrate can transfer a significant strain field to the superconducting layer and accelerate I_c degradation in iron-based superconductors[42]. Using 1.2 MeV protons, the Bragg peak is located several microns into the substrate and assumed to have a negligible effect on the REBCO layer; see figure 1. Experiments are under way to verify this assumption. A 'deep' Bragg peak also limits the number of injected interstitials, which can change the chemistry of REBCO, or stabilize voids in the case of H and He. By using a 1200 keV proton beam, less than 0.047% of the ions are deposited in the REBCO layer. In other words, for a dose of 10^{20} protons/m^2 there are $\sim$0.25 appm-H in REBCO.

3. *In situ transport-current measurements*

The four point probe arrangement used to measure I_c and T_c is shown in the upper-left of figure 3. In this configuration, the tape is bolted to the base plate through terminal blocks (7/32 x 3/4 x 3/8 in.^{3}). Although the spring-loaded pins collect voltage across the entire tape, the voltage near I_c is almost exclusively caused by the current-limiting bridged section.

To determine I_c, the temperature is fixed while I_{op} (operating current) is increased. An IV measurement begins by stabilizing the sample temperature. Next, a thermal voltage offset is measured from the average of 20 values obtained at $I_{op} = 0$ A. The current is then increased in small steps, and measured by a Keithley DMM6500 digital multimeter over a 1 mΩ shunt resistor. The voltage taps, labeled V+ and V- in figure 3, sample the voltage across the superconductor which is digitized by a Keithley 2182A nanovoltmeter. The current ramp is terminated when the voltage reaches a predetermined threshold up to 50 μV. Directly fitting the IV curve to equation 1, or a straight line on a log-log plot, yields I_c and the power law exponent n. The latter procedure is known to lower the standard deviation of repeated measurements. Most importantly, $V_c > 2\delta V$, meaning that I_c is discernible from noise.

To determine T_c, the transport current is fixed while temperature is increased. A measurement starts by stabilizing temperature at a few Kelvin above, or below, $T_c \approx 88$ K for the unirradiated tape as shown in figure 6. The transport current is then fixed to 1 mA, while temperature is slowly ramped across the superconducting transition at a rate of 0.5 K/min. To exclude thermal voltages, we report the average of the voltage values measured with current flowing in the forward and reverse directions. The prescribed ramp rate offers a reasonable measurement time (10-20 min) and alignment between the upward-ramp and downward-ramp curves within the typical temperature fluctuation of CX-T, indicating that the REBCO temperature is in quasi-equilibrium. The simplest definition of T_c is given by the maximum of first derivative of voltage with respect to temperature.

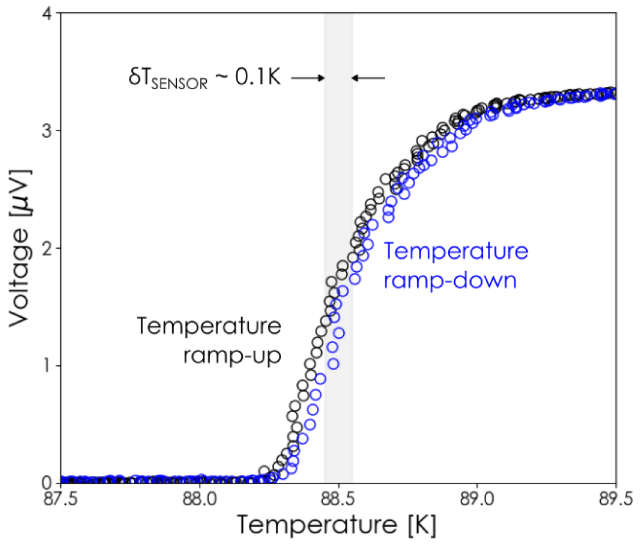

FIG. 6. Critical temperature measurement (0.5 K/min, $I_{op} = 1\,mA$) showing a typical temperature noise level $\delta T < 0.1$ K, allowing measurements of T_c with the same precision.

4. *Data acquisition and hardware control*

The data acquisition and control system (DAC) is based on serial communication between a Linux desktop computer and the voltage, current and temperature measurement devices. Two power supplies, also controlled by serial communication, run current through the tape. The first is a Lakeshore 121 Current Source ($\pm$ 100 nA up to 100 mA), used to measure T_c. The second is a Keithley 2231-A power supply which provides up to 6 A in steps as small as 1 mA. This power supply also provides control voltage to an HP6260B current source, that can provide up to 100 A in steps of 0.3 A. Altogether, this system can apply transport currents from 100 nA to 100 A, spanning nine orders of magnitude. The DAC is orchestrated by a custom-built PyQt5 graphical user interface (GUI) implementing the pyserial library to comunicate with the serial ports. The temperature and tape-voltage signals are shielded by DB25 shielded-cables, from inside the target-holder to the measurement devices, where data is acquired at a rate of 3 points/s. In addition to reading voltage and temperature, the GUI provides remote control of vacuum pumps and cryocooler using a Numato Lab 32 Channel USB Relay Module. Further, the user can pre-define measurement sequences to run automated data acquisition routines. This software solution is complemented by a quench protection system (QPS): a hardware fail-safe that can cut off the current supplied to the sample in $\sim$1 ms to avoid damage in case of a quench. The QPS circuit consists of an instrumentation amplifier, low-pass and notch filters, and a window comparator. The comparator outputs a 12 V logic level into a D flip-flop, which activates the gate driver of a high-power transistor used to cut off the current. At the cut off condition the flip-flop is immediately cleared, and remains in this state until the circuit is reset by the DAC. A schematic of the QPS is shown in figure 7.

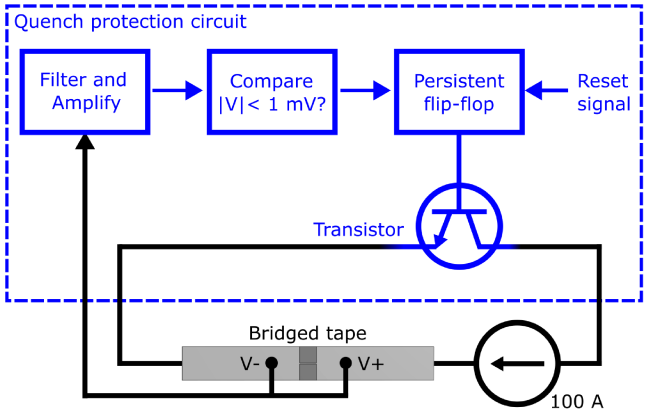

FIG. 7. Block diagram of the quench protection system, which can cut off the current supplied to the sample in $\sim$1 ms to avoid damaging the sample in case of a quench.

IV. FIRST RESULTS

A. Influence of irradiation temperature

Figure 8 shows preliminary results demonstrating the effect of different irradiation temperatures on I_c. Two pairs of REBCO tape samples were cut from the same spool and irradiated with 1.2 MeV protons, measuring I_c at 20 K after each fluence step. The flux was kept between 12-15×10^{16} protons/m^{2}s, except for the tape plotted with open blue squares, where dose rate was 5 times slower. The blue tapes, irradiated at 20 K, degrade significantly faster than their red counterparts, irradiated at 300 K. This data is compatible with the following explanation: at low temperatures, radiation-induced defects are frozen in place and preserved; while at high temperatures, thermal energy facilitates defect mobility and a larger fraction of Frenkel-pairs can recombine.

B. Thermal annealing after cryogenic irradiation

Figure 9 shows the evolution of I_c in a tape irradiated at 21 K, where the post-irradiation temperature is increased in steps of 3 K. For each step, the temperature is ramped at a rate of approximately 7 K/min, and held constant at the anneal temperature for one hour. Each point is obtained by averaging 8 measurements (taken at 21 K, 0 T). In this specific instance, where the tape had lost 8% of its unirradiated I_c, we find an onset of annealing effects at $\sim$150 K. Our facility also has the ability to investigate the time-dependence of annealing by sending milisecond pulses with amplitudes of several hundreds of amps. This causes Joule heating in the silver layer, warming the REBCO for very short periods of time[43]. Since thermal-cycles will occur during the maintenance of fusion and HEP devices, a better understanding of annealing mechanisms can be leveraged to maximize I_c recovery and, thus, magnet lifetime.

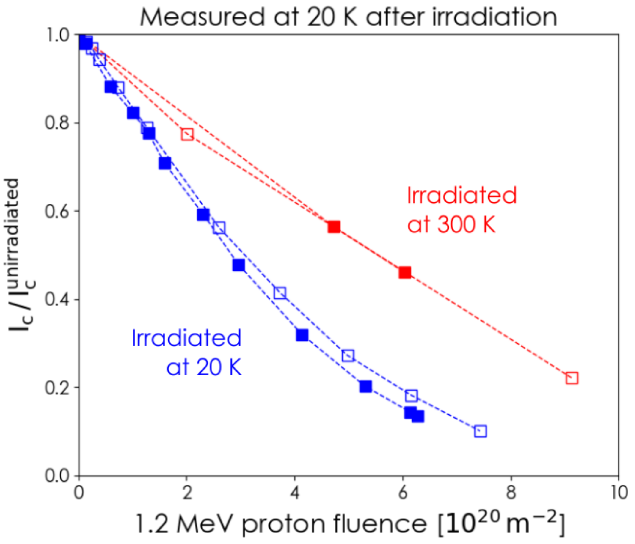

FIG. 8. Cryogenic irradiation causes a faster degradation of I_c than room temperature irradiation since defects are more mobile at 300 K than 20 K, and thus recombine more easily. In this experiment, four identical samples were irradiated with 1.2 MeV protons at a typical flux density of 12-15 $\times 10^{16}$ m^{-2}s. Each marker is the average of 3 measurements and the error bars are smaller than the markers.

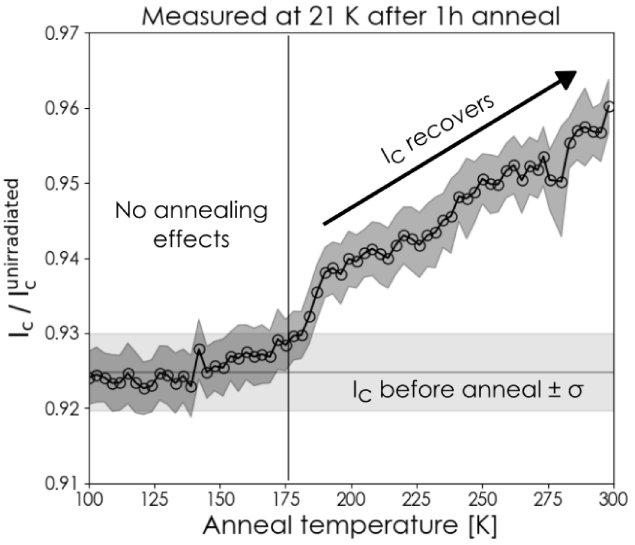

FIG. 9. Isochronal anneal steps carried out after irradiation at 21 K show that the critical current (21 K, 0 T) starts to recover well-below room temperature. In this figure, markers are the average of 8 measurements with a standard deviation indicated by the envelope.

C. Prompt suppression of I_c during irradiation

Finally, by applying transport current during irradiation, our facility can investigate the performance of REBCO in a radiation-field. For instance, figure 10 shows a significant increase in voltage at a fixed $I_{op}/I_c = 1.14$, which appears and disappears as the beam is steered on and off the sample. While

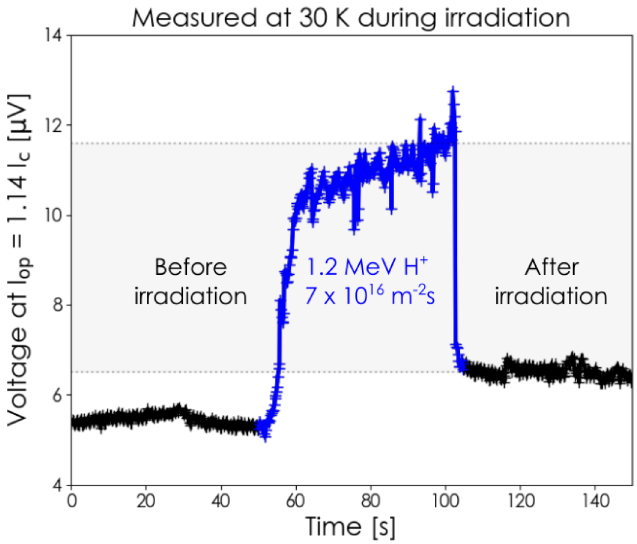

FIG. 10. An instantaneous recovery of the critical current is observed when the beam is steered away from the sample, as indicated by an immediate drop in voltage. The higher baseline recorded after irradiation is likely due to the accumulation of stable defects.

ongoing research at MIT points to a predominant role of localized beam heating, alternative hypotheses have been proposed by the community to explain the beam-on effect. These include the breaking of Cooper pairs by direct Coulombic interactions from the incident particle[44], or the large dynamic population of defects present during the ballistic stage of the damage cascade. Clarifying the extent to which beam heating can explain the beam on suppression of I_c is important to determine if, e.g., a given flux of neutrons could perturb the steady-state operation of fusion magnets.

V. FACILITY UPGRADES

Two efforts are presently under way to extend radiation damage studies of REBCO tapes at MIT, and complement the capabilities of the cryogenic ion-irradiation facility.

The first extension is the planned addition of a compact, REBCO-based, split pair magnet providing *in-situ* I_c(B, T, θ) measurements at magnetic fields up to 10 T and magnetic-field-angles ranging from 0 to 180°. This upgrade will extend our critical measurements to the range where transport behavior is dominated by external magnetic fields and scaling laws can be used to confidently extrapolate our results to the high-field magnet performance range[45]. Another key objective of this upgrade is to further explore the impact of radiation damage on the I_c anisotropy regarding magnetic field direction. Previous ex-situ results have shown that medium fluences degrades the B ∥ ab peak in $I_c(\theta)$ and raises the B ∥ c levels, flattening the $I_c(\theta)$ dependence and eliminating the anisotropic effects of strong external pinning centers used by REBCO manufacturers and exploited by magnet designers[35,46].

The second extension is the construction of a new facility

for cryogenic fast-neutron irradiation of magnet materials at the MIT Reactor (MITR-II), a 6 MW research reactor located on main campus. The new facility targets relevant neutron fluences at cryogenic temperatures, with and without transport current, and with *in-situ* $I_c(B,T,\theta)$ characterization. To achieve its target, the facility will make use of a unique capability of MITR-II known as a fast fission convertor, in which thermal neutron beams are incident on ex-core ^{235}U leading to fission and the emission of a Watt energy spectrum of neutrons which peaks around 1 MeV and extends up to $\sim$8 MeV. The fast neutrons are emitted into a cubic meter of atmospheric space, adjacent to the reactor, in which the cryogenic irradiation facility will be built without the challenges of in-core engineering and with a larger experimental room where a 14 T Nb_3Sn magnet will be installed for $I_c(B,T,\theta)$ characterization. Importantly, the cryogenic irradiation of bulk magnet-relevant materials beyond REBCO, including other superconductors such as Bi2212 but also metals, insulation, solders, and instrumentation, are also planned for this facility as well as detailed proton-neutron irradiation similarity studies to better understand the radiation damage mechanisms and understand under what conditions proton irradiation can serve as a proxy for the more resource-intensive neutron irradiation.

VI. CONCLUSION

A facility for the characterization of REBCO tapes under ion-irradiation is available at the MIT Plasma Science and Fusion Center. The *in-situ* capability, i.e., cryogenic irradiation followed immediately by I_c measurement without an intermediate warm-up step, is essential to preserve the radiation-induced defect landscape within the REBCO layer, and evaluate its consequences on the superconducting properties of the tape. Three demonstration measurements of REBCO tapes were presented: (1) the impact of irradiation temperature on the degradation of I_c; (2) onset temperature for annealing-recovery; and (3) the prompt suppression of I_c which appears and disappears as the beam is steered on and off the sample. Each of these measurements carries new physical insights into the radiation tolerance REBCO, and bears important consequences for the design and operation of large-scale magnets in fusion, HEP and space applications. Combining the cryogenic ion-irradiation setup described in this paper with the upcoming cryogenic neutron irradiation facility will provide an unprecedented capability to study the behavior of REBCO tapes in radiation-intense applications. On the one-hand, ion-irradiations deliver rapid, low-cost, and experimentally flexible capabilities with a variety of species, energies, and *in-situ* characterization techniques. Neutron irradiations, on the other hand, offer the highest fidelity irradiation and testing of REBCO tapes for fusion magnets. Both facilities are poised to deliver new scientific insights into cuprate superconductors, as well as better design criteria and operational certainty for large-scale REBCO magnets a radiation field.

VII. DATA AND MATERIALS AVAILABILITY

The cryogenically irradiated REBCO tapes are available upon reasonable request to MPS. All data needed to evaluate the conclusions in this paper can be accessed directly at the repository (https://doi.org/10.5281/zenodo.11002961).

VIII. ACKNOWLEDGEMENTS

This work was supported by Eni S.p.A. through the MIT Energy Initiative. ARD is grateful to Vadim Amelichev (S-Innovations) and Alexander Molodyk (Faraday Factory Japan) who kindly provided coated-conductor samples for our research; to J.L. Cheng for continued access to the laser-skiver at Commonwealth Fusion Systems; to Lauryn D Kortman and Zoe L Fisher for their help and dedication to maintaining and improving the facility; and to the accelerator gods for blessing our target chamber with big bright beautiful beams during the experimental campaign of 2022-2023.

[1] A. Molodyk, S. Samoilenkov, A. Markelov, P. Degtyarenko, S. Lee, V. Petrykin, M. Gaifullin, A. Mankevich, A. Vavilov, B. Sorbom, J. Cheng, S. Garberg, L. Kesler, Z. Hartwig, S. Gavrilkin, A. Tsvetkov, T. Okada, S. Awaji, D. Abraimov, A. Francis, G. Bradford, D. Larbalestier, C. Senatore, M. Bonura, A. E. Pantoja, S. C. Wimbush, N. M. Strickland, and A. Vasiliev, "Development and large volume production of extremely high current density YBa2Cu3O7 superconducting wires for fusion," Scientific Reports **11**, 1–11 (2021).

[2] D. G. Whyte, J. Minervini, B. LaBombard, E. Marmar, L. Bromberg, and M. Greenwald, "Smaller & Sooner: Exploiting High Magnetic Fields from New Superconductors for a More Attractive Fusion Energy Development Path," Journal of Fusion Energy **35**, 41–53 (2016).

[3] A. J. Creely, M. J. Greenwald, S. B. Ballinger, D. Brunner, J. Canik, J. Doody, T. Fülöp, D. T. Garnier, R. Granetz, T. K. Gray, and et al., "Overview of the sparc tokamak," Journal of Plasma Physics **86**, 865860502 (2020).

[4] A. Sykes, A. Costley, C. Windsor, O. Asunta, G. Brittles, P. Buxton, V. Chuyanov, J. Connor, M. Gryaznevich, B. Huang, J. Hugill, A. Kukushkin, D. Kingham, A. Langtry, S. McNamara, J. Morgan, P. Noonan, J. Ross, V. Shevchenko, R. Slade, and G. Smith, "Compact fusion energy based on the spherical tokamak," Nuclear Fusion **58**, 016039 (2017).

[5] J. Alonso, I. Calvo, D. Carralero, J. Velasco, J. García-Regaña, I. Palermo, and D. Rapisarda, "Physics design point of high-field stellarator reactors," Nuclear Fusion **62**, 036024 (2022).

[6] D. Endrizzi, J. Anderson, M. Brown, J. Egedal, B. Geiger, R. Harvey, M. Ialovega, J. Kirch, E. Peterson, Y. Petrov, and et al., "Physics basis for the wisconsin hts axisymmetric mirror (wham)," Journal of Plasma Physics **89**, 975890501 (2023).

[7] K. Ferrone, C. Willis, F. Guan, J. Ma, L. Peterson, and S. Kry, "A review of magnetic shielding technology for space radiation," Radiation **3**, 46–57 (2023).

[8] M. Evans and A. Ignatiev, "Using lunar superconducting magnetic energy storage (lsmes) for nasa artemis program," in *Lunar Surface Innovation Consortium (LSIC): Low Temperature Sub-kW Power and Energy Storage for the Lunar Surface* (NASA Technical Management, 2022) pp. 1–2.

[9] B. Sorbom, J. Ball, T. Palmer, F. Mangiarotti, J. Sierchio, P. Bonoli, C. Kasten, D. Sutherland, H. Barnard, C. Haakonsen, J. Goh, C. Sung, and D. Whyte, "Arc: A compact, high-field, fusion nuclear science facility and demonstration power plant with demountable magnets," Fusion Engineering and Design **100**, 378–405 (2015).

[10] L. Bottura, S. A. Gourlay, A. Yamamoto, and A. V. Zlobin, "Superconducting magnets for particle accelerators," IEEE Transactions on Nuclear Science **63**, 751–776 (2016).

[11] B. W. Kleiner R, *Superconductivity: An Introduction* (Wiley-VCH Verlag GmbH & Co. KGaA, Boschstr. 12, 69469 Weinheim, Germany, 2016).

[12]en*Handbook of Superconductivity: Fundamentals and Materials, Volume One*.

[13]W. K. Kwok, U. Welp, A. Glatz, A. E. Koshelev, K. J. Kihlstrom, and G. W. Crabtree, "Vortices in high-performance high-temperature superconductors," Reports on Progress in Physics **79**, 116501 (2016).

[14]K. Tsuchiya, X. Wang, S. Fujita, A. Ichinose, K. Yamada, A. Terashima, and A. Kikuchi, "Superconducting properties of commercial rebco-coated conductors with artificial pinning centers," Superconductor Science and Technology **34**, 105005 (2021).

[15]R. Unterrainer, D. X. Fischer, A. Lorenz, and M. Eisterer, "Recovering the performance of irradiated high-temperature superconductors for use in fusion magnets," Superconductor Science and Technology **35**, 04LT01 (2022).

[16]S. B. L. Chislett-McDonald, L. Bullock, A. Turner, F. Schoofs, Y. Dieudonne, and A. Reilly, "In-situ critical current measurements of rebco coated conductors during gamma irradiation," Superconductor Science and Technology **36**, 095019 (2023).

[17]S. Chromik, C. Camerlingo, M. Sojkova, V. Strbik, M. Talacko, I. Malka, I. Bar, G. Bareli, and G. Jung, "Low energy electron beam processing of ybco thin films," Applied Surface Science **395**, 42–49 (2017), progress in Applied Surface, Interface and Thin Film Science and Solar Renewable Energy News IV.

[18]D. X. Fischer, R. Prokopec, J. Emhofer, and M. Eisterer, "The effect of fast neutron irradiation on the superconducting properties of REBCO coated conductors with and without artificial pinning centers," Superconductor Science and Technology **31** (2018).

[19]A. A. Soman, S. C. Wimbush, N. J. Long, M. W. Rupich, C. Notthoff, P. Kluth, J. Leveneur, J. Kennedy, and N. M. Strickland, "Reduced critical current anisotropy and improved critical current performance in a combined pinning landscape created by proton and silver irradiation," IEEE Transactions on Applied Superconductivity **33**, 1–5 (2023).

[20]G. S. Was, *Fundamentals of Radiation Materials Science* (Springer, 2016).

[21]M. Frischherz, M. Kirk, J. Farmer, L. Greenwood, and H. Weber, "Defect cascades produced by neutron irradiation in yba2cu3o7Δ," Physica C: Superconductivity **232**, 309–327 (1994).

[22]Y. Linden, W. Iliffe, G. He, M. Danaie, D. Fischer, M. Eisterer, S. Speller, and C. Grovenor, "Analysing neutron radiation damage in yba2cu3o7x high-temperature superconductor tapes," Journal of Microscopy **286**, 3–12 (2022).

[23]Y. Jiang, Z. Chen, Y. Han, P. Deb, H. Gao, S. Xie, P. Purohit, M. W. Tate, J. Park, S. M. Gruner, V. Elser, and D. A. Muller, "Electron ptychography of 2D materials to deep sub-ångström resolution," Nature **559**, 343–349 (2018).

[24]R. J. Nicholls, S. Diaz-Moreno, W. Iliffe, Y. M. Linden, D. A. Tayebeh, M. Mohsen, C. R. M. Grovenor, and S. C. Speller, "Understanding irradiation damage in high-temperature superconductors for fusion reactors using high resolution x-ray absorption spectroscopy," Communications Materials (2022).

[25]A. Yabuuchi, T. Ozaki, H. Sakane, H. Okazaki, H. Koshikawa, S. Yamamoto, and T. Yamaki, "Characterization of the effect of ion irradiation on industrially produced gdba2cu3o7 superconducting tapes using a slow positron beam," Applied Physics Express **13**, 123004 (2020).

[26]R. Auguste, M. O. Liedke, M. Butterling, B. P. Uberuaga, F. A. Selim, A. Wagner, and P. Hosemann, "In situ measurements of non-equilibrium positron state defects during He irradiation in Si," Journal of Applied Physics **133**, 185901 (2023).

[27]B. S. Brown, R. C. Birtcher, R. T. Kampwirth, and T. H. Blewitt, "Resistivity and Tc measurements in low temperature irradiated Nb3Sn and Nb3Ge," Journal of Nuclear Materials **72**, 76–82 (1978).

[28]P. A. Hahn and M. W. Guinan, "A Cryogenic System for Fusion Neutron Irradiation and In-Situ Measurements on Superconductors," in *Advances in Cryogenic Engineering*, edited by R. W. Fast (Springer US, Boston, MA, 1988) pp. 639–646.

[29]I. Mukouda and Y. Shimomura, "Effects of low-temperature neutron irradiation on tc of lnba2cu3o7-y (ln = y, la) and la2cuo4," Japanese Journal of Applied Physics **30**, 2744–2746 (1991).

[30]H. Gerstenberg and W. Gläser, "Neutron irradiations at temperatures below 6 k at the munich research reactor (frm)," Nuclear Science and Engineering **110**, 50–55 (1992).

[31]P. Müller, W. Schindler, G. Saemann-Ischenko, H. Burzlaff, H. Gerstenberg, and M. Fischer, "Neutron irradiation of yba2cu3o7 and y1.2ba0.8cuox," Physica C: Superconductivity **153-155**, 343–344 (1988).

[32]S. A. Davydov, B. N. Goshchitskii, A. E. Karkin, A. V. Mirmelshtein, V. I. Voronin, M. V. Sadovskii, V. L. Kozhevnikov, S. V. Verkhovskii, and S. M. Cheshnitskii, *Advances in Superconductivity*, edited by K. Kitazawa and T. Ishiguro, Vol. 1 (Springer Japan, 1989) pp. 463–468.

[33]H. Wiesinger, F. Sauerzopf, H. Weber, H. Gerstenberg, and G. Crabtree, "Flux pinning by collision cascades and large defect clusters in single crystal yba2cu3o7," Europhysics Letters **20**, 541 (1992).

[34]B. Egner, J. Geerk, H. C. Li, G. Linker, O. Meyer, and B. Strehlau, "The influence of irradiation-induced defects on the superconductivity of yba2cu3o7," Japanese Journal of Applied Physics **26**, 2141 (1987).

[35]B. N. Sorbom, *The Effect of Irradiation Temperature on REBCO Jc Degradation and Implications for Fusion Magnets*, Ph.D. thesis, Massachusetts Institute of Technology (2017).

[36]W. Iliffe, N. Peng, G. Brittles, R. Bateman, R. Webb, C. Grovenor, and S. Speller, "In-situ measurements of the effect of radiation damage on the superconducting properties of coated conductors," Superconductor Science and Technology **34** (2021).

[37]S. R. Foltyn, L. Civale, J. L. Macmanus-Driscoll, Q. X. Jia, B. Maiorov, H. Wang, and M. Maley, eng"Materials science challenges for high-temperature superconducting wire," Nature Materials **6**, 631–642 (2007).

[38]Benkel, Tara, Miyoshi, Yasuyuki, Chaud, Xavier, Badel, Arnaud, and Tixador, Pascal, "Rebco tape performance under high magnetic field," Eur. Phys. J. Appl. Phys. **79**, 30601 (2017).

[39]K. Tang, *Evaluation of Novel Laser-Skived Microbridges for Improved Characterization of REBCO Superconductor*, Master's thesis, Massachusetts Institute of Technology (2023).

[40]J. F. Ziegler, M. Ziegler, and J. Biersack, "Srim the stopping and range of ions in matter (2010)," Nuclear Instruments and Methods in Physics Research Section B: Beam Interactions with Materials and Atoms **268**, 1818–1823 (2010), 19th International Conference on Ion Beam Analysis.

[41]M. Short, D. Gaston, M. Jin, L. Shao, and F. Garner, "Modeling injected interstitial effects on void swelling in self-ion irradiation experiments," Journal of Nuclear Materials **471**, 200–207 (2016).

[42]D. Torsello, M. Fracasso, R. Gerbaldo, G. Ghigo, F. Laviano, A. Napolitano, M. Iebole, M. Cialone, N. Manca, A. Martinelli, L. Piperno, V. Braccini, A. Leo, G. Grimaldi, A. Vannozzi, G. Celentano, M. Putti, and L. Gozzelino, "Proton Irradiation Effects on the Superconducting Properties of Fe(Se,Te) Thin Films," IEEE Transactions on Applied Superconductivity **32**, 1–5 (2022).

[43]Z. L. Fisher, *Annealing Cryogenically Irradiated High TemperatureSuperconductors with Current Pulses*, Master's thesis, Massachusetts Institute of Technology (2023).

[44]W. Iliffe, K. Adams, N. Peng, G. Brittles, R. Bateman, A. Reilly, C. Grovenor, and S. Speller, "The effect of in situ irradiation on the superconducting performance of reba$_2$cu$_3$o$_7$ δ -coated conductors," MRS Bulletin (2023).

[45]C. Senatore, C. Barth, M. Bonura, M. Kulich, and G. Mondonico, "Field and temperature scaling of the critical current density in commercial rebco coated conductors," Superconductor Science and Technology **29**, 014002 (2015).

[46]N. M. Strickland, S. C. Wimbush, A. A. Soman, P. Kluth, C. Notthoff, R. Knibbe, M. Li, and M. W. Rupich, "Isotropic and anisotropic flux pinning induced by heavy-ion irradiation," IEEE Transactions on Applied Superconductivity **32**, 1–5 (2022).